Simple synthesis of novel Lanthanum doped Copper oxide nanoparticles for wastewater treatment: A comparison between Experiment and COMSOL simulation

Arslan Masood
University of Gujrat - Hafiz Hayat Campus: University of Gujrat
Tahir Iqbal (tiqbal02@qub.ac.uk)
University of Gujrat - Hafiz Hayat Campus: University of Gujrat https://orcid.org/0000-0001-9211-7342
Sumera Afsheen
University of Gujrat - Hafiz Hayat Campus: University of Gujrat
Khalid Riaz
University of Okara
Ghulam Nabi
University of Gujrat - Hafiz Hayat Campus: University of Gujrat
Muhammad Isa Khan
University of Gujrat - Hafiz Hayat Campus: University of Gujrat

Research Article

Keywords: Photocatalysis, CuO-NPs, La doepd CuO-NPs, Solgel method, MB dye, COMSOL Mltiphysics

Posted Date: January 25th, 2022

DOI: https://doi.org/10.21203/rs.3.rs-937180/v1

Abstract

Photocatalysis is a promsing technique for remediation and decontamination of waste water. This research work focuses on the synthesis of pure and lanthanum (La)- (1, 2 and 3 wt%) doped copper oxide nanoparticles (CuO-NPs) via a simple, cost effective and efficient sol-gel process. Differnet characterization techniques such as UV-vis, PL, SEM, XRD, EDS and FTIR are used to investigate optical, compositonal, structural and morphological properties of the synthesized material. Quite interestingly, doping of rare earth element La has reduced the particle size (52.02 ± 0.04 nm to 42.39 ± 0.02 nm) of CuO-NPs. Additionaly, with doping, the band gap and electron hole recombiantion rate is also reduced. Band gap has shifted towards visible region (3.13 ev to 2.85 ev) which makes it an excellent mateiral for photocataysis. Methylene blue (MB) dye is used as model contamination. Photocatalytic degradation efficieny of 79% is obtained in 150 min by $La_{0.02}Cu_{0.98}O$ against MB under natural light irrradiation. Band gap is increased upon futher doping which attributes to the reduced catalytic efficiency to 73% for $La_{0.03}Cu_{0.97}O$. Theoratical photocatalytic activity of CuO-NPs against MB dye with particle size of 50nm is carried out using COMSOL Multiphysics 5.3a Licenced version in order to corelate the experimental and theoratical results.

1. Introduction

Organic dyes are the most widely used compounds in industries due to their ability to resist fading when exposed to light, perspiration, water, oxidising agents, and microorganisms (Arunadevi et al., 2018; Saratale, Saratale, Chang, & Govindwar, 2011). Due to their widespread use and large-scale manufacturing, dyes are now found in considerable quantities in wastewater (Kazeminezhad & Sadollahkhani, 2014). Roughly 1–15 percent of synthetic textile dyes are estimated to be dumped into effluents during the manufacturing process (Shahabuddin et al., 2018). These dyes are released directly into water bodies, which caused substantial water contamination owing to their carcinogenic nature (Kumar & Pandey, 2017). Due to their enormous moelcular size and complicated structures, the majority of these dyes are hazardous and non-biodegradable and thus can result in major risks and threats to aquatic and human life (Tanwar, Kumar, Mandal, & Chemistry, 2017). Researchers are wokring hard to overcome this problem using different scientific methods. These dyes are removed via a range of physical, chemical and biological processes such as adsorption, precipitation, ozonisation (Saeed & Khan, 2017). Many of these techniques are non-destructive, insufficient and produce secondary contamination. Furthermore, well-established chemical techniques are non economical. Moreover, aerobic decontamination is inefficient for stable dyes, while anaerobic oxidation process of dyes results in the formation of carcinogenic aromatic amines (Nezamzadeh-Ejhieh & Khorsandi, 2010). Numerous sophisticated oxidation processes, notably sonocatalysis, ozonolysis, photo-Fenton, photocatalysis and photo electro-Fenton, have emerged as promising techniques for degrading toxic chemicals from wastewater (Kansal, Sood, Umar, Mehta, & Compounds, 2013). Modern photocatalysis uses heterogeneous semiconductors to degrade organic dyes/pollutants in water. Metal nanoparticles (NPs) are employed as heterogeneous photocatalysts in this method. TiO2 (Gupta et al., 2007; Kansal et al.,

2013), ZnO (Ullah et al., 2015), BiVO4 (Chomkitichai et al., 2019), WO3 (Khan, Khan, Usman, Imran, & Saeed, 2020), Fe2O3 (Abhilash, Akshatha, & Srikantaswamy, 2019) and copper-based NPs have all been reported as potential heterogeneous photocatalysts (Gu, Chen, Chen, Zhou, & Parsaee, 2018).

Copper is one of the most inexpensive metal and has a diverse range of applications, including gas sensors (Mikami, Kido, Akaishi, Quitain, & Kida, 2019), lithium-ion batteries (Ha, Kim, & Choi, 2020; Lin et al., 2017), field emission devices (Banerjee & Joo, 2011), antibacterial agents (Mary, Ansari, & Subramanian, 2019), dye-sensitized solar cells (Cao et al., 2017), adsorption (BATOOL, QURESHI, HASHMI, MEHBOOB, & DAOUSH, 2019; Salehi et al., 2016) and heterogeneous catalysts (Marcelo, Puiatti, Nascimento, Oliveira, & Lopes, 2018; T. Zhang, Souza, Xu, Almeida, & Asefa, 2018). Additionally, copper-based compounds have recently been discovered to be helpful in a variety of photocatalytic applications, including the photoconversion of toxic hydrocarbons into harmless molecules (Arunadevi et al., 2018). Copper-based semiconductors do seem to have a small band gap that can be precisely tuned by using different methods to harvest wide range of natural/synthetic radiation (Salavati-Niasari & Davar, 2009). They were thus extensively employed as a strong heterogeneous photocatalyst. Since the electrons in the conduction band are unstable in phase pure CuO, the majority of the photogenerated electrons migrate to the valance band and recombine with the hole without engaging in the oxidation process (Sonia et al., 2015). This implies that by postponing the recombination of charge carriers in photocatalysis, the overall efficiency of the reaction can be enhanced. Different methods were used to decelerate the photogenerated electron-hole recombination in CuO including surface modification, rare eath and transition metal doping (Abu-Zied, Bawaked, Kosa, & Schwieger, 2016; Devi et al., 2017; Ekthammathat, Phuruangrat, Thongtem, & Thongtem, 2016; Meshram, Adhyapak, Mulik, & Amalnerkar, 2012). Doping of rare earth elements in CuO is one of the most effective method because it can delay the recombination rate of photogenerated charge carriers by introducing localised impurities/defect states near the velance band or the conduction band (or both) which can trap the electrons to enhance photocatalytic efficineicy (Devi et al., 2017). Furthermore, rare-earth elements have been found to decrease the bandgap of CuO, which permits faster charge carriers transition across the forbidden gap, reducing the recombination rate (Abu-Zied et al., 2016).

Nanoparticle preparation methods are significant for determining their properties. CuO NPs can be synthesized using a range of methodologies, including the sol-gel technique (Kayani, Umer, Riaz, & Naseem, 2015), co-precipitation (Vidyasagar, Naik, Venkatesh, & Viswanatha, 2011), hydrothermal method (X. Zhang, Zhang, Ni, & Zheng, 2008), green synthesis (Sutka & Mezinskis, 2012), solid state reaction (Singh & Bedi, 2011), sono-chemical method (Muhammad R Islam, Rahman, Farhad, Podder, & Interfaces, 2019), thermal decomposition (Muhammad R Islam et al., 2020) etc. Among them, the sol-gel method provides a convenient, efficient, simple, and cost-effective route for the synthesis of NPs that involves a self-sustaining reaction in a solution of various oxidizers.

In the present study, pure and La doped CuO nanoparticles have been synthesised using a facile sol-gel method. Analyses of the structural and optical characteristics of the nanoparticles as they were produced were carried out using FTIR, XRD, SEM, PL and UV–vis spectroscopy. Additionally, the impact of the La

content on the NPs' photocatalytic activity was examined experimentally. The findings indicate that incorporation of La lowers the band gap of the CuO NPs, thus improving their photocatalytic activity. COMSOL 5.3a Licensced version is used to construct a 2D model of this research work to simulate photocatalytic degradation of MB dye by CuO-NPs in order to study corelation between experiment and simulation.

2. Materials And Methodolgy

2.1. Chemicals

Copper nitrate ($Cu(NO_3)_2.3H2O$) and Lanthanum nitrate($La(NO_3)_3.6H2O$), respectively, were used as precursors for Cu and La. Deionized (DI) water (18 M.cm) is used as solvent. Citric acid served as chelating agent in the reaction. Amonia (NH_3) solution is used to control the pH. All the chemicals used in this research work are 99% pure from sigma Aldrich.

2.2. Method

Sol-gel process is adopted for the synthesis of pure and La (1, 2, 3 wt%) doped CuO-NPs. Aqueous solution of 0.5M copper nitrate and 0.5M citric acid are prepared separately, then stirred at room temperature for 30 minutes to get a homogenous solution. Once dissolved, the stock solution is made by combining the two solutions in a glass beaker while stirring at 50°c. The pH of the solution was adjusted to 9 by adding an adequate quantity of NH3 solution drop wise. The temperature is gradually increased to 90°C. After 2 hours of continuous stirring, a thick brownish black gel is produced at the bottom of the beaker which is washed and dried in the oven. After finely grounding, it is calcinated at 550°C for two hours to obtain NPs of pure CuO. Lanthanum nitrate solution of different concentrations (1, 2 & 3 %) was combined with citric acid and copper nitrate solution to synthesizeLa:CuO NPs. Hence, a formulation procedure identical to that used to produce CuO nanoparticles was followed. The flow chart of the procedure is shown in figure 1.

2.3. Characterizations

Following the nanoparticle synthesis, their physical characteristics and photocatalytic activity were evaluated. The lattice parameters, bond angles, bond lengths and crystalline size of the NPs were determined using the X-ray diffraction (XRD) method. XRD was performed using an X-ray diffractometer (KAPPA Apex II) and CuKα radiation with a wavelength of 1.5406 Å. Surface morphology of synthesized samples is studied using a Field emission scanning electron microscope (FE-SEM) (TESCAN MIRA 3). Fourier transform infrared spectroscopy (FTIR) using a (FT/IR-4100-A Jasco) spectrophotometer with a spectral range of 500-4000 was used for the chemical analysis. Photoluminescence (FP-8200, JASCO) and UV-vis (UV/1700, Shimadzu) spectroscopy is used to study the optical properties of synthesized pure and La doped CuO-NPs.

2.4. Photocatalytic activity

Photocatalytic activity of synthesized pure and La doped CuO-NPs against MB dye, under natural light irradiation was analyzed. In this experiment, 200ml of 1 *ppm* solution of MB and 20mg of fine powder photocatalyst (pure CuO and La 1, 2 & 3% doped CuO-NPs respectively) were taken. Measurement period of catalytic activity was set to be 150 min. In order to achieve absorption-desorption equilibrium between catalyst and dye, the suspension was stirred in the dark for one hour. Subsequently, this suspension was exposed to natural light irradiation and the reading was taken after every 30 min until 150 min. The color of suspension was shifted from blue to colorless. UV-visible spectrometer was used to analyze the residual solution. Intensity of UV peak at 570 nm was directly related to the MB (%) left in the suspension. Percentage degradation was calculated using the following formula (A. Muthuvel, M. Jothibas, & C. J. N. f. E. E. Manoharan, 2020).

$$\text{Degradation}(\%) = \frac{C_0 - C_t}{C_0} \times 100\% \quad (1)$$

Here, initial absorption is represented by C_0 and C_t indicates absorption after various time intervals. Degradation percentage for all samples is evaluated over 150 min.

2.5. COMSOL 5.3(a)

Analytic or numeric approach used in mathematical modeling is very beneficial for solving real-life based physical problems. Out of these two, numeric approach is preferred since a computer can efficiently handle any type and size of data as compared to humans. Finite elemental analysis (FEA) has been used in structural mechanics and it is reported in 1940's (Courant & mathematics, 1994). As a way to have a superior concept of the collaboration of electromagnetic (EM) waves by the Nano based, a commercial FEA software program bundle, COMSOL 5.3a Licensed version, with RF module, is mostly elaborated to construct the 2D model essential for this study work. FEA involves the easy and quick understanding of interaction between EM waves and sub-wavelength device (CuO in this case). This technique enables us to split the whole computation space into finite size elements on which further approximation could be solved.

The geometry of the model is generated by sketching multiple sub-domains in COMSOL using various tools and settings to represent different materials and areas. Schematic diagram of the model is illustrated in figure 8(a). Three types of boundary conditions are utilized in this model namely: continuity boundary conditions (CBCs), scattering boundary conditions (SCBs) and periodic boundary conditions (PBCs). The CBCs are applied to internal sides of structure to ensure continuity of tangential components of the electromagnetic field whereas the PBCs are applied on the external boundaries to approximate a large structure by considering the unit cell. The SCBs are used to reduce the reflection (Ghosh & Palik, 1997). Perfectly matched layers (PMLs) are another kind of condition that may be used to limit the interior of the computation region. These PMLs are used when the scattering boundaries are not adequately absorbing the incident fields owing to the wave vector's dispersion. These conditions are applied to the rear of the internal continuity boundaries, thus extending the computation domain to half

the incident wavelength. When a certain domain is designated as PML, the two subsequent domains act in the same way i.e., the interface of two domains does not present any obstructions to the incoming wave. The wave emerges in the next domain exactly as it is, with no energy loss or modification (Iqbal, 2013).

The sub-domain at the bottom is referred to as the excitation port or in-port. This indicates that the model's input power is supplied vertically upward at this port. The value of the input power supplied at this port may be adjusted to any optimal value from the global expression, such as 12700 watts in present case. Additionally, the harmonic propagation mode is an essential clause in the current model. Meshing is a very important step of solving the model. The physical domains are divided into smaller sub-domains of irregular geometry defined as element. The element serves as the fundamental unit of the discretization process in order to get the solution. In a model, the elements of each subdomain are connected to one another via points, known as nodes.

Model parameters are fixed to conduct a sweep for variables. The model's most often used parameter is wavelength, which spans from 400nm to 1000nm and is configured to vary in 1nm increments. TM-polarized light may get the necessary information through transmission, reflection, or absorption at different angles. The last step is to set the parametric solver to sweep the model's variables. The wavelength range (400-900nm) is crucial in this simulation. The model is irradiated by s and p-polarized light at a constant angle (0°).

3. Results And Discussion

3.1. XRD analysis

The phase composition and crystalline structure of CuO and La: CuO NPs were investigated through their XRD patterns. The variation of the XRD pattern for CuO and La:CuO-NPs is depicted in figure 2(a). At the 2 θ value = 32.59, 35.58, 38.78, 48.91, 53.56, 58.37, 61.65, 66.32 and 68.20, the diffraction peaks correspond to the crystal planes (110), (-111), (111), (-202), (020), (202), (113), (311) and (221), verifying the monoclinic structure of CuO-NPs. There are no visible diffraction peaks from any of the other copper oxide phases. The recorded XRD pattern matches with phase pure CuO from JCPDS Card no. 01-080-1268 (Gopinath et al., 2016).

It can be seen from the XRD profile that the CuO NPs are highly crystalline, as shown by the sharp and intense diffraction peaks. It can be seen in figure 2(b) that the intensity of diffraction peaks decreases as the concentration of La increases, indicating that the crystalline structure has been deteriorated as a result of doping. Peak of lanthanum oxide or lanthanum hydroxide is absent in the XRD pattern. The concentration of La caused a slight change in XRD peaks. The atomic radius difference between La3+ (106 pm) and substituted Cu2+ (73 pm) may cause this change (Xing et al., 2017). A shift in the diffraction peak shows doping of the CuO lattice with La ions. The Scherer equation was used to determine the crystallite size of the NPs (A. Muthuvel, M. Jothibas, & C. J. J. o. E. C. E. Manoharan, 2020).

$$D = \frac{0.9\lambda}{\beta Cos\theta}$$

2

Where β represents full width half maxima (FWHM), θ is the Bragg's diffraction angle and λ is X-ray wavelength (1.5406 Å). In Fig. 3b, the size of CuO and La:CuO nanoparticles is shown to be decreased with the increasing concentration of La dopant. The crystallite size evaluated by equation (2) is 52.02 ± 0.04, 47.58 ± 0.05 and 42.39 ± 0.02nm for pure and La (1 & 2%) doped CuO-NPs. The decrease in NP crystallite size is due to the creation of La–O–Cu bonds by La doping. La-doped ZnO showed similar dopant-induced modifications in NP crystallite size (Anandan et al., 2007).

3.2. Morphological and Compositional analysis

Surface morphology and compositional analysis of CuO and La:CuO-NPs is carried out by scanning electron microscope (SEM) and energy dispersive spectroscopy (EDS). Figure 3 (a,b) & (c,d) exhibits the SEM micrographs and the EDS mapping of the synthesized material respectively. Pure CuO-NPs have irregular morphology and the EDS analysis indicates the absence of any impurity element. However, the 2% La doped CuO-NPs has agglomeration and EDS spectrum reveals the homogeneous distribution of dopant element over the surface of host material. Moreover, the particle size for doped sample is reduced as compared to pure material. It attributes to the fact that particle growth is inhibited due to the presence of rare earth metal La (Muhammad Rakibul Islam et al., 2021).

3.3. Optical studies

The photoluminescence (PL) and ultraviolet visible spectroscopy (UV-vis) is used to investigate the optical properties of fabricated pure and La doped CuO-NPs. Characteristic peak of CuO at 268nm and 452nm is present. Absorption peak of 452nm attributes to the plasmon resonance band and atomic copper cluster (Sohrabnezhad, Valipour, & Spectroscopy, 2013). Band gap of synthesized pure and La doped CuO-NPs is estimated by diffuse reflectance spectroscopy. The Kubelka-Munk function F(R) relates absorption coefficient (α) to reflectance (R) by the following relation (Muhammad R Islam et al., 2020):

$$F(R) = {(1-R)^2}/{2R} = {\alpha}/{s} \quad (3)$$

Where R, s and α represents reflectance, scattering and absorption coefficient respectively. The Tauc equation relates the band gap (E_g) to the absorption coefficient (α) by:

$\alpha h\nu = A(h\nu - E_g)^n$ (4)

Where A is a constant of proportionality, hv is the incident light energy and n = 1/2 for the direct band gap. When treating the coefficient s as a constant, the F(R) can reasonably be considered proportional to α. Then the Tauc relationship in Kubelka-Munk function is rewritten (Muhammad R Islam et al., 2020):

$(\alpha h F(R))^2 = (A/s)(h\nu - E_g)$ (5)

Extrapolating the straight-line parts of the curves in the plot of $(\alpha hF(R))^2$ against hv gives the band gap of NPs. The E_g values for CuO and La:CuO-NPs were extracted from the plot as represented in figure 4(a). The band gap of pure CuO was determined to be 3.14 eV, which is consistent with the reported value. Figure 4(b) illustrates the band gap fluctuation of the NPs as a function of La concentration. The La doping was observed to reduce the band gap of NPs. This decrease in band gap may be attributed to the presence of impurity states between the CuO's conduction and valance bands due to La doping. As the number of dopant atoms increases, these impurity states coalesce near the conduction band's lowermost edges, reducing the gap between the conduction and valance bands (Rajendran et al., 2016). For 1 and 2% doping of La, band gap has reduced to 3.07 and 2.85 eV respectively but when dopant concentration is increased to 3%, the band gap increases to 3.01 eV. Burstein-Moss (BM) effect is thought to be responsible for this rise in band gap (Tiss et al., 2019). A highly doped semiconductor allows the Fermi level to migrate closer to the conduction band, resulting in an increase in the band gap. As a result, the valance band electron must expend more energy to get to an unoccupied state of the conduction band, causing the band gap to expand (Litter, Navio, & Chemistry, 1996).

The PL spectra illustrated in figure 4(c) are obtained on exciting wavelength of 335nm. Generally, the PL spectra consist of two main regions: UV region (band gap confirmation) and broad band spectrum (characteristic peaks and defects) (Marami, Farahmandjou, & Khoshnevisan, 2018). The spectrum has two characteristic peaks located at 413 nm and 425 nm. The blue emission peak of 413 nm attributes to singly ionized copper (Cu^+) vacancies. The shoulder peak at 425 nm is associated with the surface defects of CuO-NPs due to oxygen vacancies. In pure sample, the cluster of electronic excitations is occurred which is not controlled by material itself which leads to the high rate of electron hole recombination (Sharma et al., 2017). Dopant element (La) is used to control the electron hole recombination. Drop in PL intensity confirms the reduction in the recombination rate, desirable for photocatalytic applications.

3.4. FTIR

Chemical composition and bonds of pure and La doped CuO-NPs were examined by Fourier Transformation Infrared (FTIR) Spectroscopy. Figure 4(d) depicts typical spectrum of CuO and La:CuO-NPs recorded between 500-4000 cm^{-1}. In the FTIR spectrum, absorption bands at 598, 759, 795, 878, 1054, 1109, 1624, 2160, 3490 and 3568 cm^{-1} were present. Doping causes variation in intensity and position of the FTIR peaks which attributes to the fact that bond strength has been changed. It also confirms the successful doping of La in CuO host lattice. Absorption band around 598 cm^{-1} is the stretching vibration of CuO. Greater stretching attributes to the presence of oxygen vacancies. The presence of strong vibrational peaks at 759 cm^{-1}, 795 cm^{-1} and 878 cm^{-1} are due to C-H and C=C bond (Nabila, Kannabiran, & biotechnology, 2018). Stretching vibration bands at 1054 cm^{-1} is due to C-O whereas the bands detected near 1108 cm^{-1} and 1624 cm^{-1} are related to C=O and C-O respectively. Stretching band at 2160 cm^{-1} corresponds to the CO_2 present in the air which owes to the measuring circumstances. Peaks depicted around 3490 cm^{-1} and 3568 cm^{-1} are related to the O-H stretching

(Gnanavel, Palanichamy, Roopan, & Biology, 2017). Quit interestingly as the dopant concentration is increased, peak intensity is also enhanced. Besides the absorption bands discussed above, no impurity peak has been identified which confirms that the synthesized samples are highly pure.

Photocatalytic Analysis

Photocatalytic activity is performed by employing 20mg of the synthesized pure and La (1,2 & 3%) doped CuO-NPs as photocatalyst respectively in order to degrade 10 *ppm* aqueous solution of MB dye under natural light irradiation for 150 min. Photocatalytic degradation is observed by recording UV-vis spectrum from 450 to 750nm at various intervals of time 0, 30, 60, 90, 120 and 150 min as illustrated in figure 5. Absorption band around 670nm indicates the amount of MB dye left undegraded in the solution. Decrease in the UV-vis absorption band indicates the successful degradation of MB dye.

Photocatalytic analysis has revealed that degradation efficiency for pure and La (1, 2 & 3%) doped CuO-NPs is 51, 67, 79 and 73 % respectively as shown in figure 7(a). Photocatalytic efficiency has been improved for La doped samples. Maximum catalytic efficiency is observed for 2% La doped CuO-NPs. Intrinsically, photocatalytic efficiency depends upon the surface to volume ratio of nano photocatalyst, absorption of irradiated light and electron hole recombination rate. Smaller size of photocatalyst ensures the large surface area available for redox reaction. Photocatalytic reaction is initiated by the absorption of light of suitable frequency dictated by the band gap. Therefore, it is beneficial to reduce the band gap of photocatalyst by adding some percentage dopant impurity. Absorption of light generates photo electron hole pair. The CuO-NPs have high rate of electron hole recombination rate. Dopant impurity improves the recombination rate which facilitates the photocatalytic degradation.

It has been discussed in the SEM and XRD results that the particle size is reduced by the addition of dopant. The PL results revealed that electron recombination rate is controlled efficiently by increasing the dopant concentration. On the other hand, band gap calculated from the UV-vis spectrum shows anomaly. Band gap of pure CuO-NPs is 3.14 eV which is reduced upon doping. For 1 and 2% doping of La, band gap has reduced to 3.07 and 2.85 eV respectively but when dopant concentration is increased to 3%, Burstein Moss effect comes into play and increase the band gap to 3.01 eV. Although for 3% doped sample, electron hole recombination rate and particle size have optimal values to be a good photocatalyst but the increased energy band dominates all the other factors and photocatalytic efficiency is reduced as compared to 2% doped sample. This anomaly suggests that only a limited amount (2%) of La doping is suitable for CuO-NPs to enhance its photocatalytic activity.

3.5. Mechanism

The photocatalytic activities are often affected by variations in oxygen vacancy. The electron–hole pairs are separated based on the amount of oxygen vacancies present in the solution. According to Malleshappa *et al.* (Malleshappa et al., 2015), the photocatalytic activity varies depending on the concentration of defects at the surface level. The charge carrier recombination rate is decreased as the surface defects increases and the particle size reduces, resulting in enhanced photocatalytic activity.

Based on the observations, a plausible pathway for the photodegradation of MB dye over fabricated nanoparticles exposed to sunlight is hypothesized based on the aforementioned reaction steps:

i) Absorption of light

$$CuO + h\gamma \rightarrow e_{cb}^{-} + h_{vb}^{+}$$

ii) Production of O_2 radical

$$O_2 + e_{cb}^{-} \rightarrow \dot{O_2}^{-}$$

iii) Splitting of H_2O

$$H_2O \rightarrow H^{+} + OH^{-}$$

iv) Production of hydroxyl radicals

$$h_{vb}^{+} + OH^{-} \rightarrow OH^{*}$$

v) Neutralization reaction

$$\dot{O_2}^{-} + H^{+} \rightarrow HO_2^{*}$$

vi) Production of H_2O_2

$$2HO_2^{*} \rightarrow H_2O_2 + O_2$$

vii) Decomposition of H_2O_2

$$H_2O_2 + e^{-} \rightarrow OH^{*} + OH^{-}$$

vii) Dye degradation

$$MB + \left\{\dot{O_2}^{-}, HO_2^{*}\ or OH^{-}\right\} \rightarrow intermediate \rightarrow CO_2 \uparrow + H_2O + mineralsalt$$

According to the mechanism, when CuO-NPs are exposed to sunlight, the valence band (VB) electrons are excited to the conduction band (CB), while an equivalent number of holes are produced in the valence band (VB). These photogenerated free electron hole pairs react with water to produce highly reactive oxidizing agents ($\dot{O_2}^{-}, HO_2^{*}\ or OH^{-}$). These radicals react with MB dye for the degradation or mineralization process. The proposed mechanism for photocatalysis by CuO and La:CuO-NPs is shown in figure 6.

3.6. Kinetic studies

Photocatalytic degradation of MB dye follows a pseudo first order kinetics.

$$ln\frac{C_0}{C_t} = -kt$$

6

Where t represents the reaction time in minutes and k indicates the apparent reaction rate constant. Initial and final concentration of aqueous MB after time t is denoted by C_0 and C_t respectively. The rate constant (k) of photodegradation of MB dye by pure CuO-NPs and La doped CuO-NPs were evaluated using equation—, and the findings are shown in Fig. 10c. BY plotting $ln(C_0/C_t)$ as a function of time (t), rate constants for pure and La (1, 2 & 3%) doped CuO-NPs is determined to be 0.00451, 0.00725, 0.01024 & 0.00811 min^{-1} whereas the fitting correlation coefficient (R^2) is found to be 0.99321, 0.98857, 0.94602 & 0.95969 respectively. Finally, it has been determined that the amount of dye degradation increases with the progression of time, as shown in figure 7(b). According to the result, 2% La doped CuO-NPs exhibited superior photocatalytic degradation of MB dye under natural light irradiation.

3.7. Photocatalytic activity via COMSOL and correlation with the experimental result

In the model, represented in figure 8(a), the size of CuO-NPs is set to be 50nm which is approximately the average size of pure CuO-NPs synthesized in this research work. This is done on purpose in order to compare the photocatalytic efficiency of experiment and simulation. Reflection (T_{ref}), transmission (T_{tran}) and absorption (T_{abs}) spectra are obtained by irradiating visible to near infrared (NIR) light shown in figure 9(a). At any wavelength, equation (7) is satisfied as shown in figure 9(a).

$$T_{abs} + T_{ref} + T_{tran} = 1$$

7

Figure 8(b) visualizes the y-component of electric field at normal incidence at 668nm wavelength. The photocatalytic activity of CuO-NPs in the prepared model is determined using MB dye. The dye degradation occurs when the model is exposed to visible to NIR light. As illustrated in figure 9(b), the degradation of dye is monitored over time by comparing their concentrations (C_t/C_0) to absorbance (A_t/A_0). The rate constant k for photocatalytic degradation of MB (n = 1.347) dye is determined and plotted in figure 9(b). Value of rate constant obtained via simulation is 0.0048 min^{-1} with fitting correlation coefficient R^2 = 0.9128.

It is observed that the rate constant for CuO-NPs obtained experimentally is very close to the theoretical value simulated with COMSOL. Experimental and theoratical values of rate constant are 0.0045 min^{-1} and 0.0052 min^{-1} respectively. For simulation, a 2D model has been considered having rigid spherical nanoparticles of 50nm. Photocatalytic activity is evaluated by considering the interaction of irradiated light in the model. Some other key factors which influence the photocatalytic reaction such as pH,

temperature, concentration of pollutant, exact morphology of material etc. are not taken into account. This may be the reason for the difference in the end result. Overall, we can say that the trend given by COMSOL is followed by the experiment.

Conclusion

A simple and cost-effective method, sol-gel is used to synthesize pure and La (1, 2 and 3%) doped CuO-NPs. The fabricated material is characterized by XRD, SEM, EDS, PL, UV-vis and FTIR to investigate the structural, compositional and optical properties. The XRD analysis revealed the monoclinic crystal structure of CuO. Moreover, with the increase in dopant concentration, the intensity of XRD peaks is decreased along with a small shift in peak position which confirms the successful doping of La. Presence of dopant also effected the crystallite size, decreasing from 52.02 $\pm$ 0.04nm to 42.39 $\pm$ 0.02nm. The UV-vis spectra depict the characteristic peak of CuO near 268nm. Tauc plot is used to extract the band gap. Doping (up to 2%) has reduced the band gap from 3.14 ev to 2.85 ev. For 3% dopant concentration, the band gap rises to 3.01 ev associated with the Burstein Moss effect. The PL analysis is used to investigate the electron-hole recombination rate. Decrease in PL intensity with doping is direct evidence of reduction in recombination rate which is a crucial parameter for photocatalysis. Purity of material is also verified by the FTIR analysis. Photocatalytic activity performed by the synthesized material against MB dye for 150 min under natural light has shown a massive improvement in degradation for doped sample as compared to the pure one. Maximum degradation of 79% is observed in 150 min by $La_{0.02}Cu_{0.98}O$. As discussed in the UV-vis section, $La_{0.02}Cu_{0.98}O$ has the minimum band gap which enables maximum absorption in the visible region. Moreover, the reduced crystallite size and electron hole recombination rate also facilitates the photocatalytic reaction. Band gap rises for $La_{0.03}Cu_{0.97}O$ retarding the photon absorption in visible region dropping the catalytic degradation efficiency to 73%. COMSOL 5.3a Licensed version is used to design the 2D model of the research work. Simulation of photocatalytic activity using perfectly spherical CuO-NPs of 50nm size against MB dye (n=1.347). Kinetic study revealed the rate constant evaluated by COMSOL is 0.0048 min^{-1} whereas the experimentally observed data for pure CuO suggests the rate constant of 0.0052 min^{-1}. The slight difference in the rate constant may be attributed to the geometry of material. Experimentally obtained CuO-NPs does not have perfectly spherical geometry (large surface area) whereas for the modelling, spherical geometry has been used. Simulation results are calculated by considering the absorption of light, completely ignoring some important parameters such as pH, temperature, morphology etc. this is the reason for the imperfection between experimental and theoretical results.

Declarations

Ethical Approval

“Not applicable”

Consent to Participate

“Not applicable”

Consent to Publish

“Not applicable”

Authors Contributions

Arslan Masood contributed about conceptualization, methodology and original/initial draft, Tahir Iqbal contributed towards conceptualization, formal analysis and Supervision, Sumera Afsheen contributed validation and review and editing, Khalid Nadeem Riaz contributed for investigation and formal analysis whereas Ghulam Nabi and Muhammad Isa Khan contributed for visualization and review of final draft.

Competing interests

"The authors declare that they have no competing interests"

Funding

“Not applicable”

Availability of data and materials

“All data generated or analysed during this study are included in this published article”

References

1. Abhilash MR, Akshatha G, Srikantaswamy SJRa (2019) Photocatalytic dye degradation and biological activities of the Fe 2 O 3/Cu 2 O nanocomposite. *9*(15), 8557–8568
2. Abu-Zied BM, Bawaked SM, Kosa SA, Schwieger WJIJES (2016) Effect of some rare earth oxides doping on the morphology, crystallite size, electrical conductivity and N2O decomposition activity of CuO catalyst. *11*, 1568–1580
3. Anandan S, Vinu A, Lovely KS, Gokulakrishnan N, Srinivasu P, Mori T,.. . Ariga KJJ o. M. C. A. C (2007) Photocatalytic activity of La-doped ZnO for the degradation of monocrotophos in aqueous suspension. *266*(1-2), 149-157
4. Arunadevi R, Kavitha B, Rajarajan M, Suganthi A, Jeyamurugan AJS, Interfaces (2018) Investigation of the drastic improvement of photocatalytic degradation of Congo red by monoclinic Cd, Ba-CuO nanoparticles and its antimicrobial activities. *10*, 32–44
5. Banerjee AN, Joo SWJN (2011) Low-macroscopic field emission properties of wide bandgap copper aluminium oxide nanoparticles for low-power panel applications. *22*(36), 365705
6. BATOOL M, HASHMI QURESHI,MZ, F., MEHBOOB, N., & DAOUSH WM (2019) AJ Csian OURNALOF HEMISTRY AJ Csian OURNALOF HEMISTRY. J A J o C 31(3):707–713

7. Cao Y, Saygili Y, Ummadisingu A, Teuscher J, Luo J, Pellet N,.. . Freitag MJN c (2017) 11% efficiency solid-state dye-sensitized solar cells with copper (II/I) hole transport materials. *8*(1), 1-8
8. Chomkitichai W, Pama J, Jaiyen P, Pano S, Ketwaraporn J, Pookmanee P,.. . Jansanthea P (2019) *Dye Mixtures degradation by multi-phase BiVO4 PhotOcatalyst.* Paper presented at the Applied mechanics and materials
9. Courant RJ L. n. i. p., & mathematics, a (1994) Variational methods for the solution of problems of equilibrium and vibrations. 1-1
10. Devi LV, Sellaiyan S, Selvalakshmi T, Zhang H, Uedono A, Sivaji K, Sankar SJA P. T (2017) Synthesis, defect characterization and photocatalytic degradation efficiency of Tb doped CuO nanoparticles. *28*(11), 3026–3038
11. Ekthammathat N, Phuruangrat A, Thongtem T, Thongtem SJML (2016) Synthesis and characterization of Ce-doped CuO nanostructures and their photocatalytic activities. *167*, 266–269
12. Ghosh G, Palik ED (1997) Handbook of Optical Constants of Solids, Five-Volume Set: Handbook of Thermo-Optic Coefficients of Optical Materials with Applications. Elsevier Science
13. Gnanavel V, Palanichamy V, Roopan SMJJ, o. P, Biology PB (2017) Biosynthesis and characterization of copper oxide nanoparticles and its anticancer activity on human colon cancer cell lines (HCT-116). *171*, 133–138
14. Gopinath V, Priyadarshini S, Al-Maleki A, Alagiri M, Yahya R, Saravanan S, Vadivelu, J (2016) In vitro toxicity, apoptosis and antimicrobial effects of phyto-mediated copper oxide nanoparticles. J R a 6(112):110986–110995
15. Gu H, Chen X, Chen F, Zhou X, Parsaee ZJU s (2018) Ultrasound-assisted biosynthesis of CuO-NPs using brown alga Cystoseira trinodis: Characterization, photocatalytic AOP, DPPH scavenging and antibacterial investigations. *41*, 109-119
16. Gupta VK, Jain R, Mittal A, Mathur M, Sikarwar SJ J. o. c., & science, i (2007) Photochemical degradation of the hazardous dye Safranin-T using TiO2 catalyst. *309*(2), 464-469
17. Ha J, Kim YT, Choi JJC (2020) In situ precipitation-induced growth of leaf-like CuO nanostructures on Cu–Ni alloys for binder-free anodes in Li-Ion batteries. *13*(2), 419–425
18. Iqbal T (2013) Nanoplasmonic grating coupler for transducer applications. Queen's University Belfast
19. Islam MR, Obaid JE, Saiduzzaman M, Nishat SS, Debnath T, Kabir AJJ, o. P, Solids C o (2020) Effect of Al doping on the structural and optical properties of CuO nanoparticles prepared by solution combustion method: Experiment and DFT investigation. *147*, 109646
20. Islam MR, Rahman M, Farhad S, Podder JJS, Interfaces (2019) Structural, optical and photocatalysis properties of sol–gel deposited Al-doped ZnO thin films. *16*, 120–126
21. Islam MR, Saiduzzaman M, Nishat SS, Kabir A, Farhad SJC, Physicochemical SA, Aspects E (2021) Synthesis, characterization and visible light-responsive photocatalysis properties of Ce doped CuO nanoparticles: A combined experimental and DFT+ U study. *617*, 126386

22. Kansal SK, Sood S, Umar A, Mehta SK J. J. o. A., & Compounds (2013) Photocatalytic degradation of Eriochrome Black T dye using well-crystalline anatase TiO2 nanoparticles. *581*, 392-397
23. Kayani ZN, Umer M, Riaz S, Naseem SJ J. o. E. M (2015) Characterization of copper oxide nanoparticles fabricated by the sol–gel method. *44*(10), 3704-3709
24. Kazeminezhad I, Sadollahkhani AJML (2014) Photocatalytic degradation of Eriochrome black-T dye using ZnO nanoparticles. *120*, 267–270
25. Khan I, Khan I, Usman M, Imran M, Saeed KJ J. o. M. S. M. i. E (2020) Nanoclay-mediated photocatalytic activity enhancement of copper oxide nanoparticles for enhanced methyl orange photodegradation. *31*(11), 8971-8985
26. Kumar A, Pandey GJMS, E. I. J (2017) A review on the factors affecting the photocatalytic degradation of hazardous materials. *1*(3), 1–10
27. Lin L, Ma Y, Xie Q, Wang L, Zhang Q, Peng D-L (2017) Copper-nanoparticle-induced porous Si/Cu composite films as an anode for lithium ion batteries. J A n 11(7):6893–6903
28. Litter M, Navio JAJJ, o. P, Chemistry PA (1996) Photocatalytic properties of iron-doped titania semiconductors. *98*(3), 171–181
29. Malleshappa J, Nagabhushana H, Sharma S, Vidya Y, Anantharaju K, Prashantha S,.. . Spectroscopy B (2015) Leucas aspera mediated multifunctional CeO2 nanoparticles: structural, photoluminescent, photocatalytic and antibacterial properties. *149*, 452–462
30. Marami MB, Farahmandjou M, Khoshnevisan BJ J. o. e. M (2018) Sol–gel synthesis of Fe-doped TiO 2 nanocrystals. *47*(7), 3741-3748
31. Marcelo CR, Puiatti GA, Nascimento MA, Oliveira AF, Lopes RP J. J. o. N. (2018). Degradation of the reactive blue 4 dye in aqueous solution using zero-valent copper nanoparticles. *2018*
32. Mary AA, Ansari AT, Subramanian RJ J. o. K. S. U.-S (2019) Sugarcane juice mediated synthesis of copper oxide nanoparticles, characterization and their antibacterial activity. *31*(4), 1103-1114
33. Meshram S, Adhyapak P, Mulik U, Amalnerkar, D J. C. e. j (2012) Facile synthesis of CuO nanomorphs and their morphology dependent sunlight driven photocatalytic properties. *204*, 158-168
34. Mikami K, Kido Y, Akaishi Y, Quitain A, Kida TJS (2019) Synthesis of Cu2O/CuO nanocrystals and their application to H2S sensing. *19*(1), 211
35. Muthuvel A, Jothibas M, Manoharan CJJ, o. ECE (2020) Effect of chemically synthesis compared to biosynthesized ZnO-NPs using Solanum nigrum leaf extract and their photocatalytic, antibacterial and in-vitro antioxidant activity. *8*(2), 103705
36. Muthuvel A, Jothibas M, Manoharan CJ N. f. E. E (2020) Synthesis of copper oxide nanoparticles by chemical and biogenic methods: photocatalytic degradation and in vitro antioxidant activity. *5*, 1-19
37. Nabila MI, Kannabiran KJB, & biotechnology, a (2018) Biosynthesis, characterization and antibacterial activity of copper oxide nanoparticles (CuO NPs) from actinomycetes. *15*, 56-62
38. Nezamzadeh-Ejhieh A, Khorsandi MJD (2010) Heterogeneous photodecolorization of Eriochrome Black T using Ni/P zeolite catalyst. *262*(1-3), 79–85

39. Rajendran S, Khan MM, Gracia F, Qin J, Gupta VK, Arumainathan SJS r (2016) Ce 3+-ion-induced visible-light photocatalytic degradation and electrochemical activity of ZnO/CeO 2 nanocomposite. *6*(1), 1-11
40. Saeed K, Khan IJTJ, o. C (2017) Efficient photodegradation of neutral red chloride dye in aqueous medium using graphene/cobalt-manganese oxides nanocomposite. *41*(3), 391–398
41. Salavati-Niasari M, Davar FJML (2009) Synthesis of copper and copper (I) oxide nanoparticles by thermal decomposition of a new precursor. *63*(3-4), 441–443
42. Salehi K, Shahmoradi B, Bahmani A, Pirsaheb M, Shivaraju HJD, Treatment W (2016) Optimization of reactive black 5 degradation using hydrothermally synthesized NiO/TiO2 nanocomposite under natural sunlight irradiation. *57*(52), 25256–25266
43. Saratale R, Saratale G, Chang J, Govindwar S (2011) Bacterial decolorization and degradation of azo dyes: a review. J Taiwan Inst Chem Eng 42:138–157. In
44. Shahabuddin S, Khanam R, Khalid M, Sarih NM, Ching JJ, Mohamad S, Saidur, R J. A. j. o. c (2018) Synthesis of 2D boron nitride doped polyaniline hybrid nanocomposites for photocatalytic degradation of carcinogenic dyes from aqueous solution. *11*(6), 1000-1016
45. Sharma A, Dutta R, Roychowdhury A, Das D, Goyal A, Kapoor AJAC, A. G (2017) Cobalt doped CuO nanoparticles as a highly efficient heterogeneous catalyst for reduction of 4-nitrophenol to 4-aminophenol. *543*, 257–265
46. Singh I, Bedi RJ S. s. s (2011) Surfactant-assisted synthesis, characterizations, and room temperature ammonia sensing mechanism of nanocrystalline CuO. *13*(11)
47. Sohrabnezhad S, Valipour AJS, A. P. A. M, Spectroscopy B (2013) Synthesis of Cu/CuO nanoparticles in mesoporous material by solid state reaction. *114*, 298–302
48. Sonia S, Annsi IJ, Kumar PS, Mangalaraj D, Viswanathan C, Ponpandian NJML (2015) Hydrothermal synthesis of novel Zn doped CuO nanoflowers as an efficient photodegradation material for textile dyes. *144*, 127–130
49. Sutka A, Mezinskis GJF, o. MS (2012) Sol-gel auto-combustion synthesis of spinel-type ferrite nanomaterials. *6*(2), 128–141
50. Tanwar R, Kumar S, Mandal UKJJ, o. P, Chemistry PA (2017) Photocatalytic activity of PANI/Fe0 doped BiOCl under visible light-degradation of Congo red dye. *333*, 105–116
51. Tiss B, Erouel M, Bouguila N, Kraini M, Khirouni KJJ, o. A, Compounds (2019) Effect of silver doping on structural and optical properties of In2S3 thin films fabricated by chemical pyrolysis. *771*, 60–66
52. Ullah Z, Rauf A, Tariq M, Tahir AA, Ayub K, Ullah HJ S. A. P. A. M., & Spectroscopy, B (2015) Phytochemical, spectroscopic and density functional theory study of Diospyrin, and non-bonding interactions of Diospyrin with atmospheric gases. *141*, 71-79
53. Vidyasagar C, Naik YA, Venkatesh T, Viswanatha RJP t (2011) Solid-state synthesis and effect of temperature on optical properties of Cu–ZnO, Cu–CdO and CuO nanoparticles. *214*(3), 337-343

54. Xing M, Sun Q, Zeng C, Wang H, Zhao D, Zhang N, Hong SJRa (2017) Modulating Cu+ distribution on the surface of Ce-doped CuO composite oxides for SO 2-resistant NH 3-selective catalytic reduction of NO. *7*(31), 18830–18837
55. Zhang T, Souza IP, Xu J, Almeida VC, Asefa TJN (2018) Mesoporous graphitic carbon nitrides decorated with Cu nanoparticles: efficient photocatalysts for degradation of tartrazine yellow dye. *8*(9), 636
56. Zhang X, Zhang D, Ni X, Zheng HJS-SE (2008) Optical and electrochemical properties of nanosized CuO via thermal decomposition of copper oxalate. *52*(2), 245–248

Figures

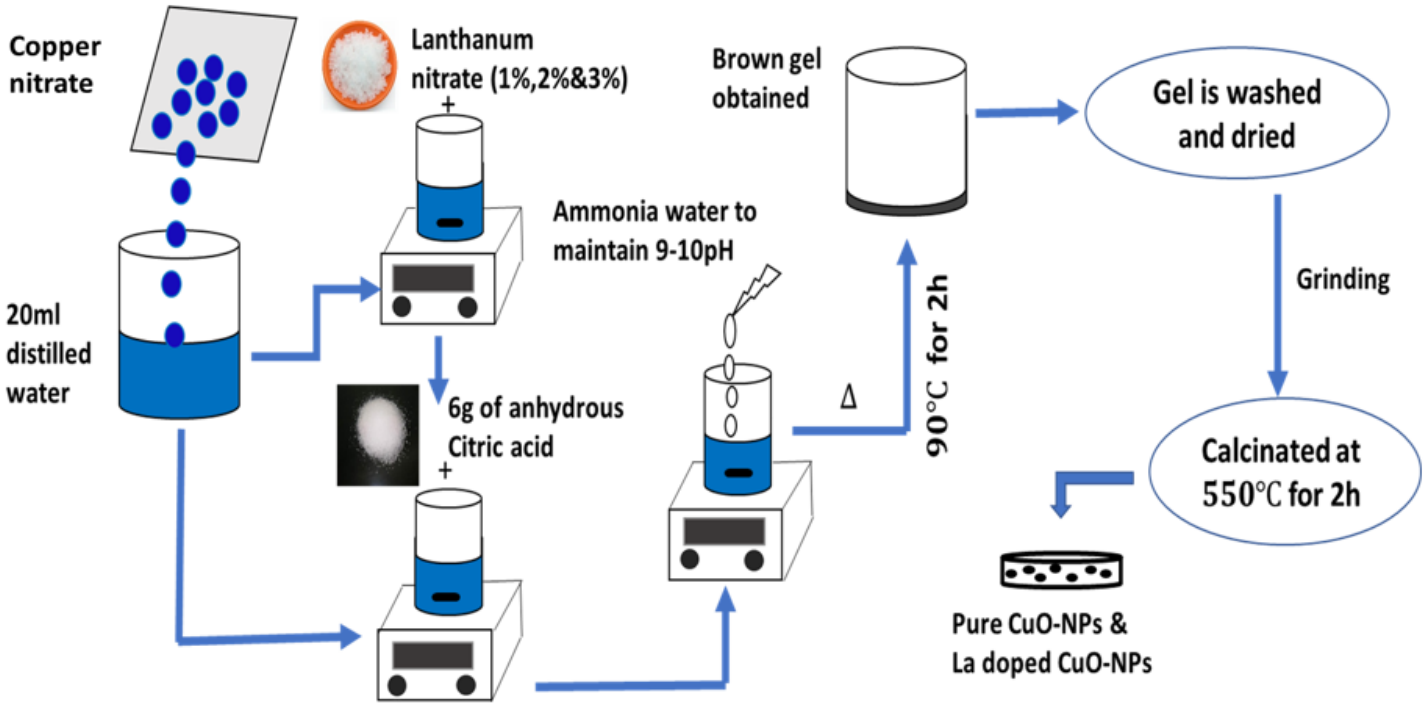

Figure 1

Flow chart of the sol-gel process to synthesize pure and La doped CuO-NPs

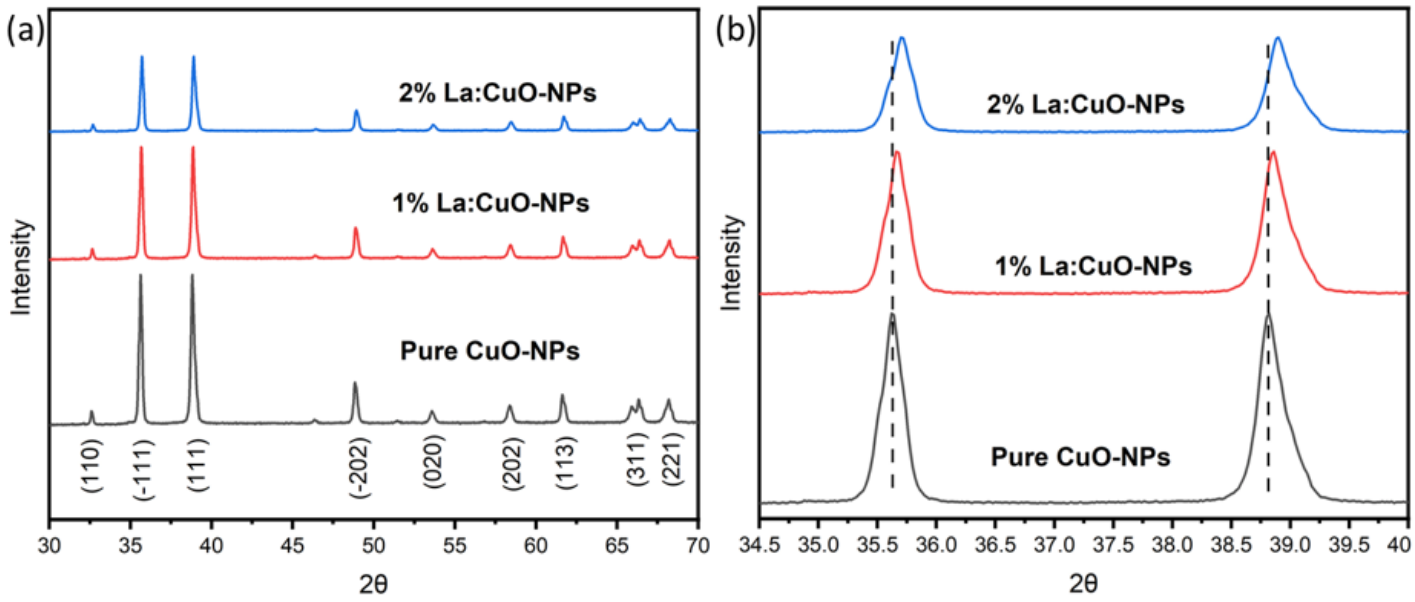

Figure 2

(a) XRD spectrum confirming monoclinic crystal structure and depicting characteristic peaks of CuO at 35.58^o and 38.78^o, (b) representing the shift and decrease in highly intense peak attributing to successful doping

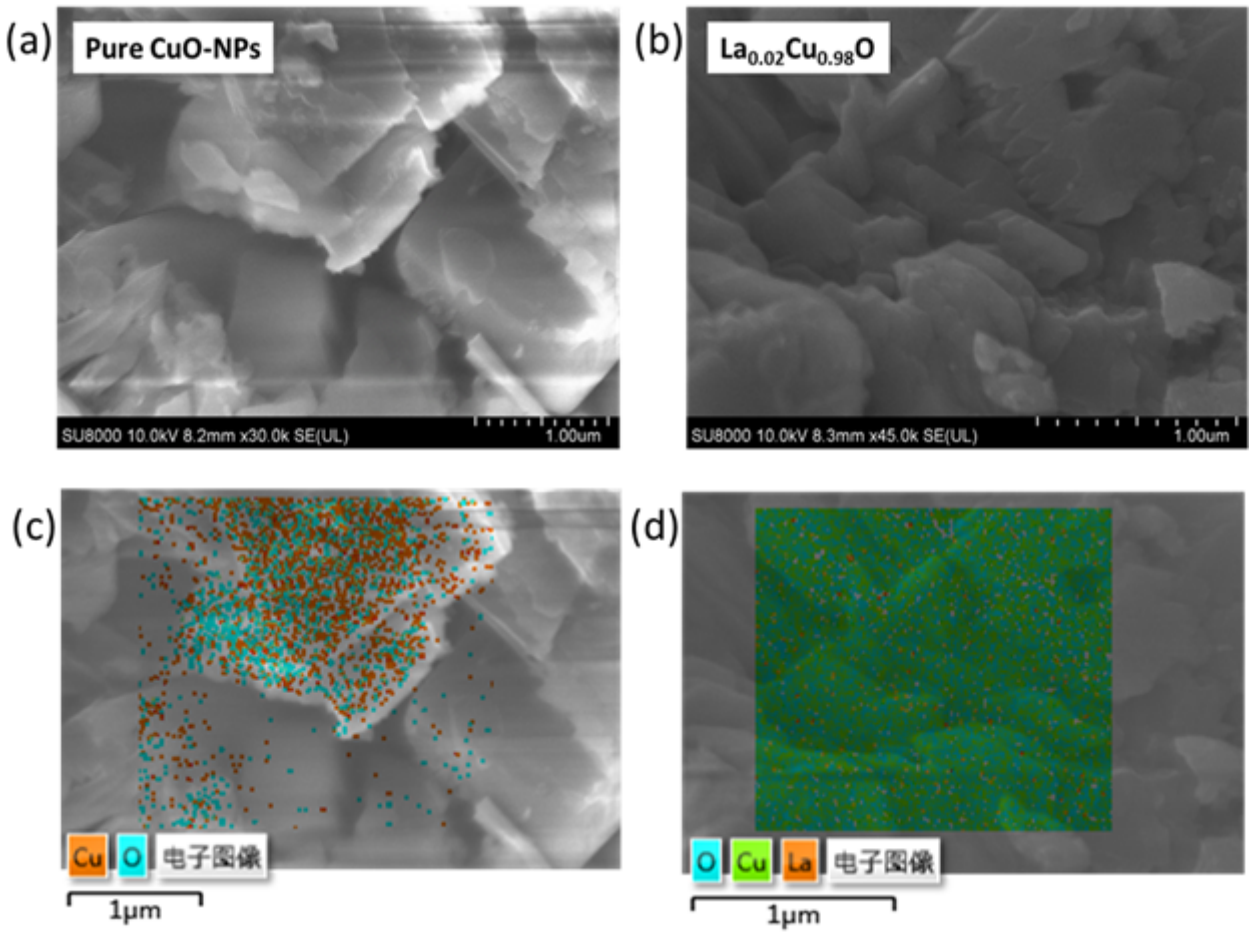

Figure 3

SEM micrographs (a) & (b) for pure and 2% La doped CuO-NPs representing irregular morphology and EDS (c) & (d) illustrates the absence of impurity for pure CuO-NPs and homogenous distribution of La for doped sample

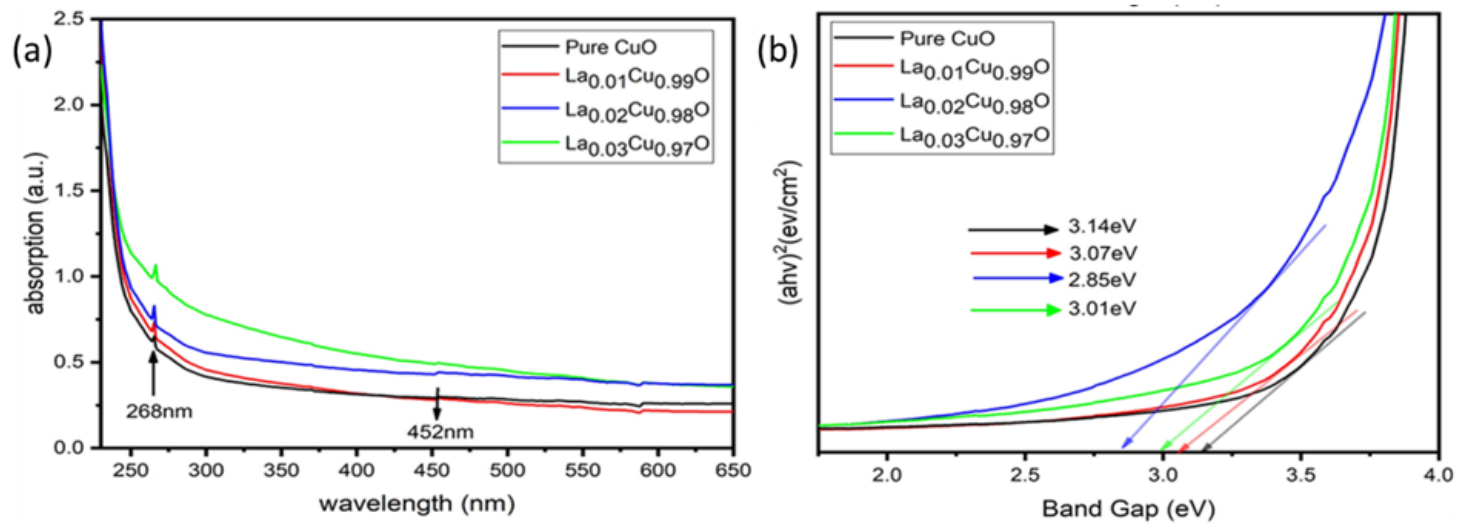

Figure 4

Characteristic peak at 268nm in UV-vis spectra (a) of pure and La doped CuO-NPs along with the corresponding Tauc plot (b) to evaluate the variation in band gap with doping concentration.

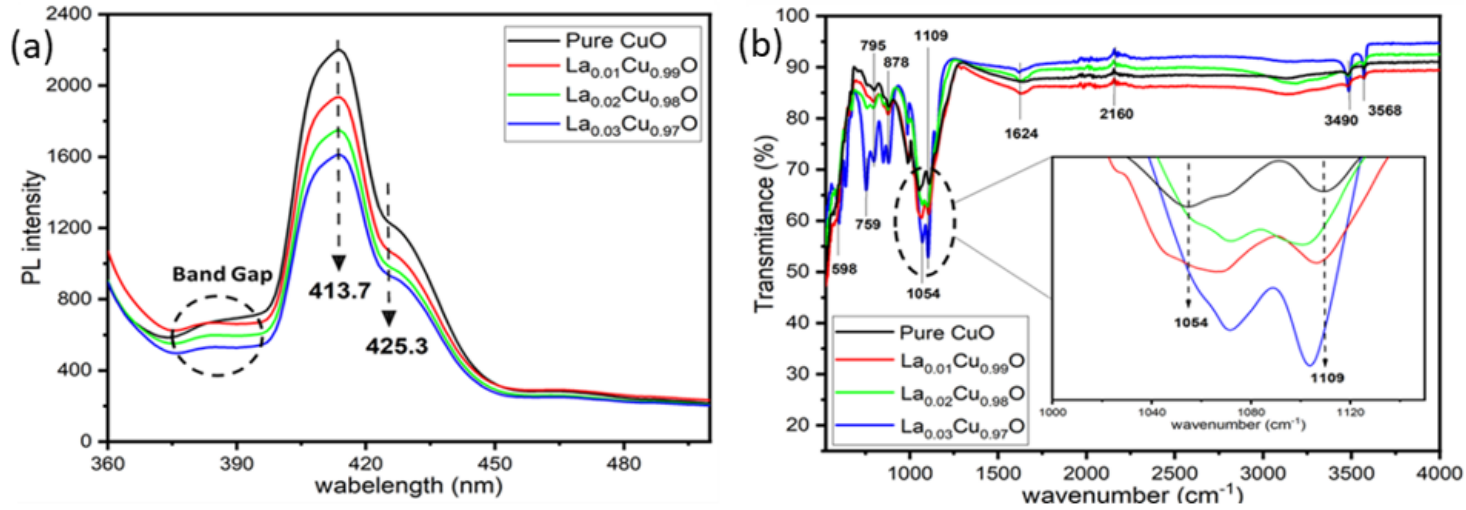

Figure 5

PL spectra (a) exhibiting reduction in highly intense peaks of 413.7nm and 425.3nm attributing to the reduced electron-hole recombination rate for doped CuO-NPs. FTIR spectra (b) of synthesized material representing a slight shift in intensity and location of peaks as shown in the inset of graph.

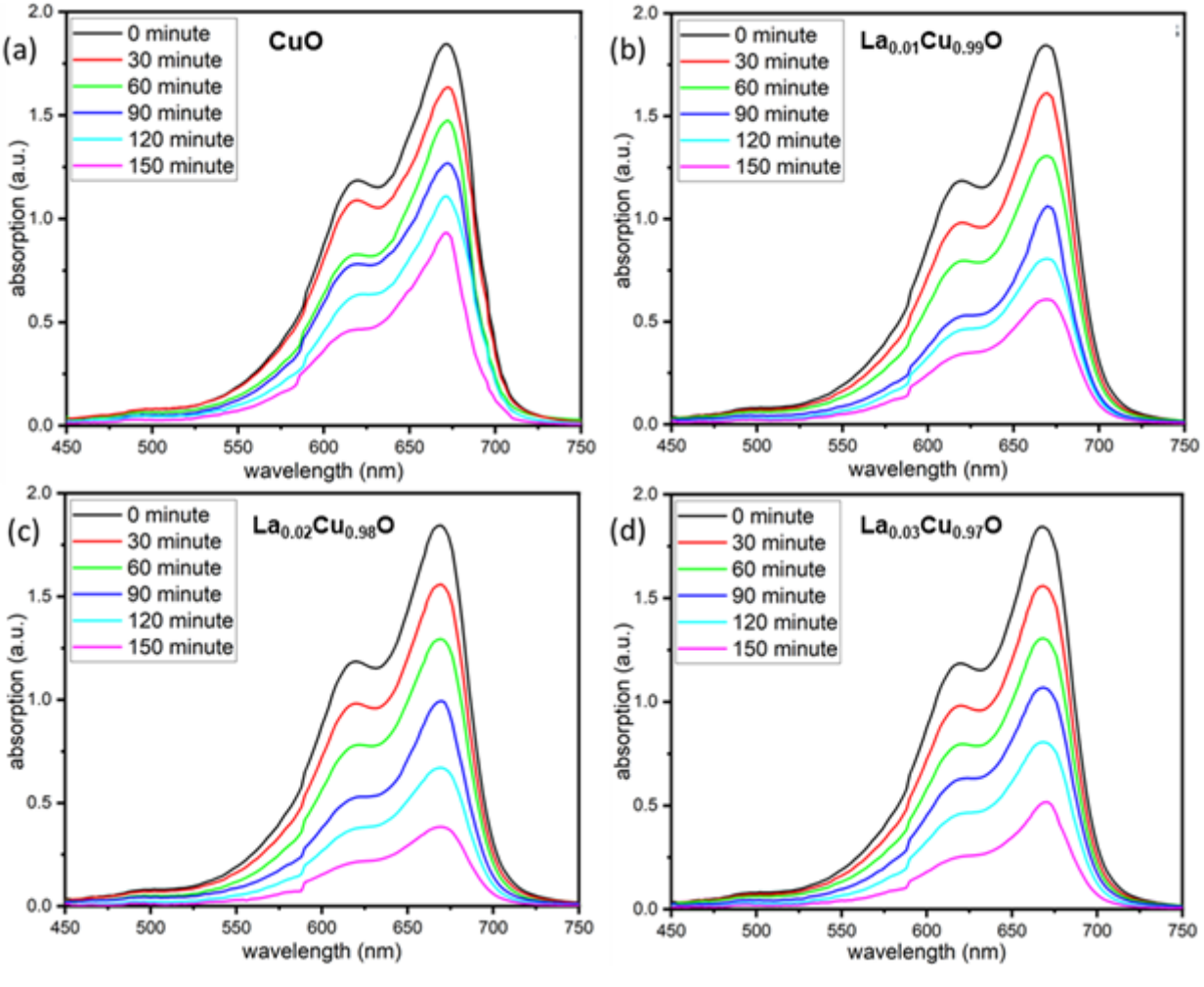

Figure 6

Photocatalytic degradation of MB dye using the synthesized pure and La doped CuO-NPs for 150 min under natural light indicating high degradation rate for doped samples.

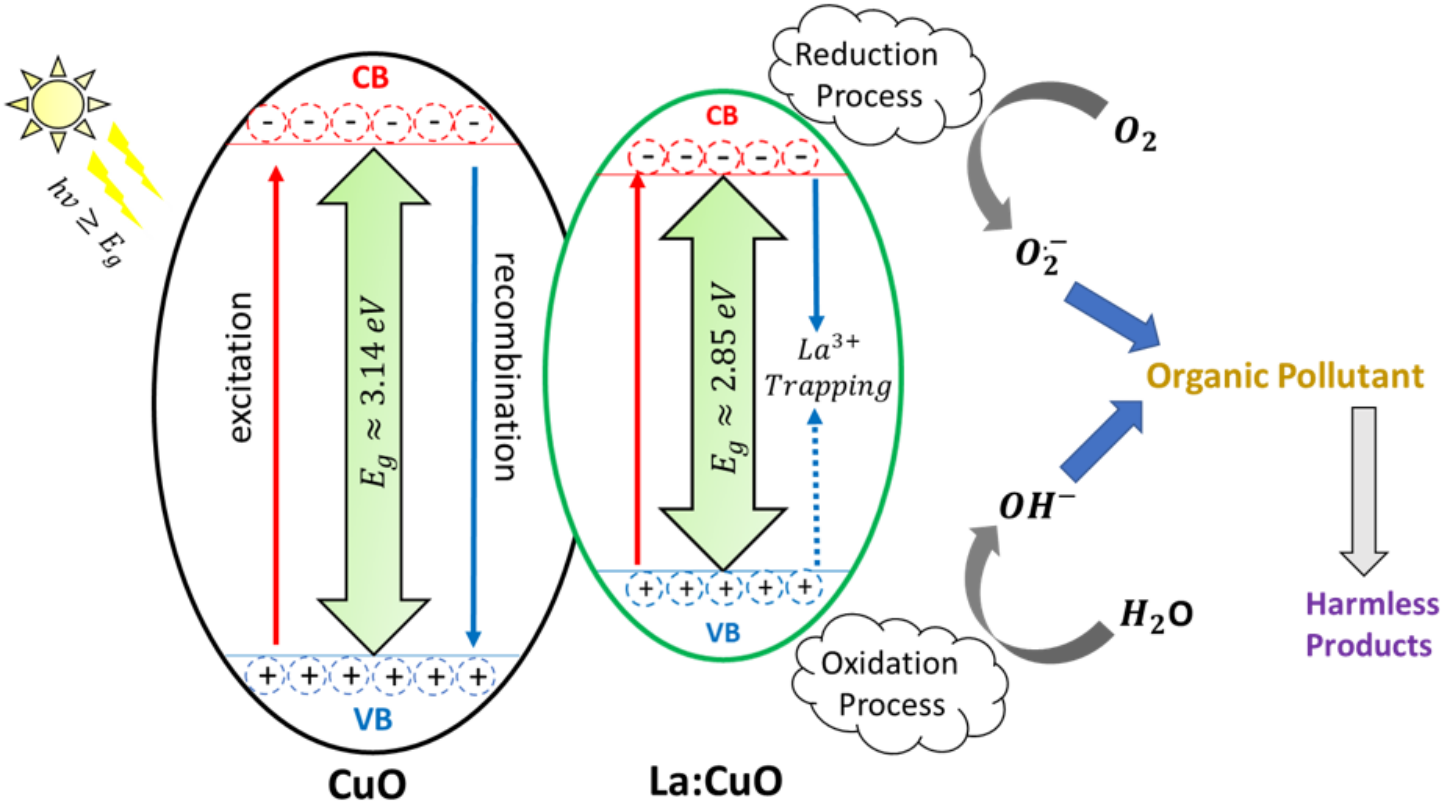

Figure 7

Mechanism of reduction in band gap and electron hole recombination rate with doping along with the free radical reaction with pollutant.

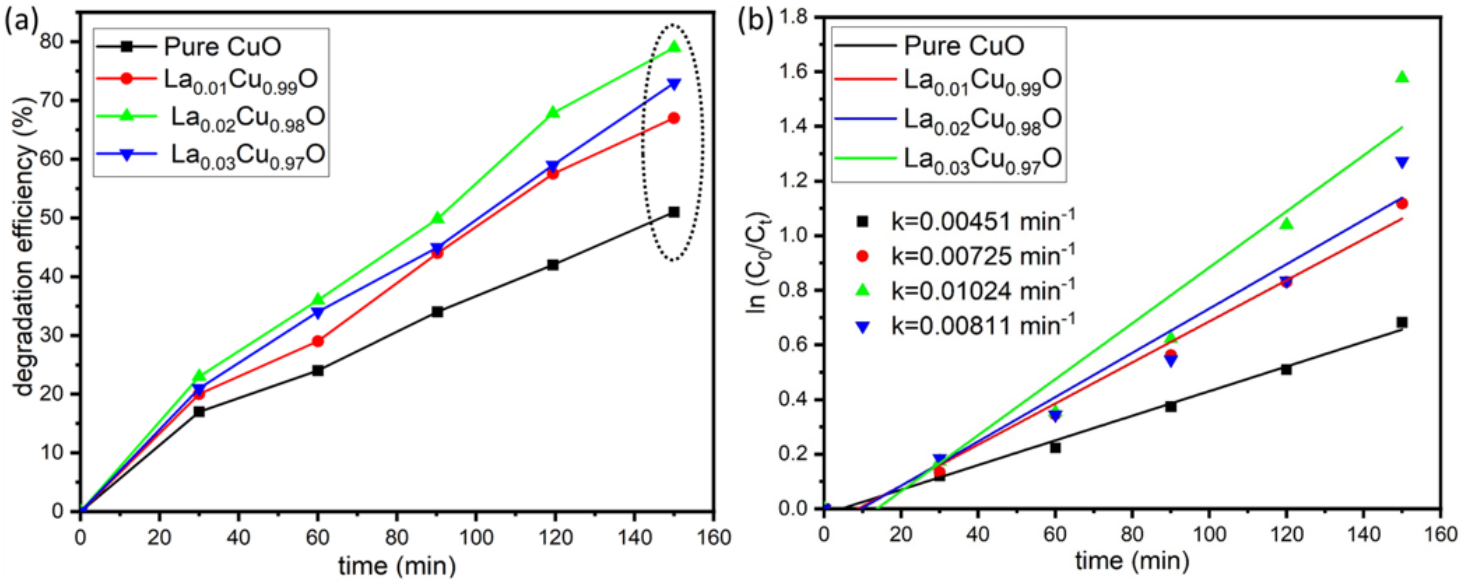

Figure 8

Photocatalytic efficiency (a) of 51%, 67%, 79%, 73% observed for pure and La (1, 2 & 3%) doped CuO-NPs along with their rate constants (b) showing variation due to the presence of dopant.

Figure 9

Schematic diagram of 2D model (a) containing immersed CuO-NPs in water. Visualization of y-component of electric field (b) at 668 nm wavelength

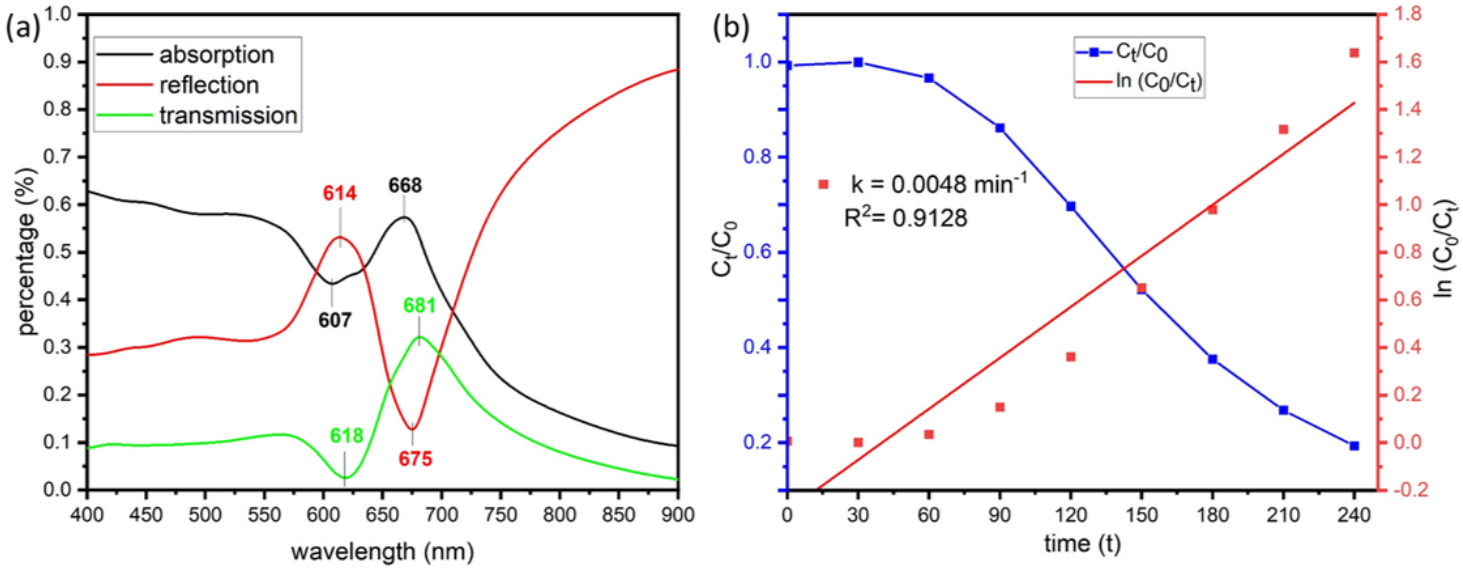

Figure 10

(a) representing the absorption, reflection and transmission of the 2D model. (b) illustrates the plot of C_t/C_0 and $ln(C_0/C_t)$ with time defining the rate constant k=0.0048 min^{-1} for COMSOL simulation of CuO-NPs against MB dye.